Appl. Math. Mech. -Engl. Ed., **42**(8), 1077–1094 (2021)

APPLIED MATHEMATICS AND MECHANICS (ENGLISH EDITION)

https://doi.org/10.1007/s10483-021-2743-6

Nonlocal vibration and buckling of two-dimensional layered quasicrystal nanoplates embedded in an elastic medium*

Tuoya SUN[1], Junhong GUO[1,2,†], E. PAN[3]

1. Department of Mechanics, Inner Mongolia University of Technology, Hohhot 010051, China;
2. School of Aeronautics, Inner Mongolia University of Technology, Hohhot 010051, China;
3. College of Engineering, Cleveland State University, Cleveland, Ohio 44115, U. S. A.

(Received Feb. 21, 2021 / Revised Apr. 13, 2021)

Abstract A mathematical model for nonlocal vibration and buckling of embedded two-dimensional (2D) decagonal quasicrystal (QC) layered nanoplates is proposed. The Pasternak-type foundation is used to simulate the interaction between the nanoplates and the elastic medium. The exact solutions of the nonlocal vibration frequency and buckling critical load of the 2D decagonal QC layered nanoplates are obtained by solving the eigensystem and using the propagator matrix method. The present three-dimensional (3D) exact solution can predict correctly the nature frequencies and critical loads of the nanoplates as compared with previous thin-plate and medium-thick-plate theories. Numerical examples are provided to display the effects of the quasiperiodic direction, length-to-width ratio, thickness of the nanoplates, nonlocal parameter, stacking sequence, and medium elasticity on the vibration frequency and critical buckling load of the 2D decagonal QC nanoplates. The results show that the effects of the quasiperiodic direction on the vibration frequency and critical buckling load depend on the length-to-width ratio of the nanoplates. The thickness of the nanoplate and the elasticity of the surrounding medium can be adjusted for optimal frequency and critical buckling load of the nanoplate. This feature is useful since the frequency and critical buckling load of the 2D decagonal QCs as coating materials of plate structures can now be tuned as one desire.

Key words two-dimensional (2D) quasicrystal (QC), nanoplate, vibration, buckling, elastic medium, exact solution

Chinese Library Classification O343
2010 Mathematics Subject Classification 52C23, 74K20, 74H45

1 Introduction

Quasicrystals (QCs)[1] are novel phases of matter which possess quasiperiodic atomic arrangements and rotational symmetries, including five-fold, eight-fold, and ten-fold symmetry

* Citation: SUN, T. Y., GUO, J. H., and PAN, E. Nonlocal vibration and buckling of two-dimensional layered quasicrystal nanoplates embedded in an elastic medium. *Applied Mathematics and Mechanics* (*English Edition*), **42**(8), 1077–1094 (2021) https://doi.org/10.1007/s10483-021-2743-6

† Corresponding author, E-mail: jhguo@imut.edu.cn

Project supported by the National Natural Science Foundation of China (Nos. 12072166 and 11862021), the Program for Science and Technology of Inner Mongolia Autonomous Region of China (No. 2021GG0254), and the Natural Science Foundation of Inner Mongolia Autonomous Region of China (No. 2020MS01006)

axes. There are two distinct types of low energy elastic excitations in QCs, i.e., phonons and phasons. According to the quasiperiodic dimension in physical space, QCs can be divided into one-dimensional (1D), two-dimensional (2D), and three-dimensional (3D) QCs. The 2D decagonal QCs considered in this paper refer to a 3D structure with atomic arrangement being periodic in one direction and quasi-periodic in the plane perpendicular to that direction. Typical 2D QCs include decagonal, octagonal, and dodecagonal ones. In 1985, the decagonal QC was firstly synthesized in the laboratory in rapidly quenched Al-Mn alloys[2–3]. By rapid solidification, Tsai et al.[4] first synthesized a decagonal phase in the Al-Ni-Fe system in 1989. In 2015, Bindi et al.[5] reported a natural QC with decagonal symmetry in the Khatyrka meteorite, and found that the natural QC had a high degree of structural perfection. Ahn et al.[6] realized a dodecagonal graphene QC by epitaxial growth of twisted bilayer graphene rotated 30°. To provide a rational design, prediction, and realization of QC formation, Liu et al.[7] developed a rational strategy to assemble 2D dodecagonal QCs from branched DNA nanomotifs. Molecular dynamics (MD) simulation is a valuable method to generate QC structures and explain the formation of QCs from the perspective of potential energy. By using double-well potentials, Chen et al.[8] obtained the decagonal and dodecagonal QCs through MD simulation.

Owing to their unique structures, QCs possess many unusual properties such as high hardness, high oxidation resistance, low frictional coefficient, low surface energy, low thermal conductivity, high wear resistance, elevated corrosion resistance, reduced wetting, and superplasticity above 700 °C, which make them attractive for technological applications such as superconductivity, photonics, coatings, and reinforced composites[9–11]. In general, synthesized QCs are at micro/nano-scale. The nano-QCs, exhibiting remarkable ductility and extraordinary specific strength at room temperature, together with interesting functional properties, may be used as structural and functional components in micro/nano-electromechanical systems[12]. Thus, nano-QCs have attracted much attention from both experimental and theoretical points of view, especially for their mechanical behaviors. Ustinov et al.[13] formed the nano-QC Al-Cu-Fe coatings by using the high rate electron beam physical vapour deposition. Using ball milling and hot extrusion, Galano et al.[14] manufactured a quasicrystalline Al alloy matrix nanocomposite containing nanoceramic particles, and found that the microhardness of the QC nanocomposite was significantly higher than both the unreinforced QC alloy and the crystalline Al nanocomposite. Pedrazzini et al.[15] found that nano-QC $Al_{93}Fe_3Cr_2Ti_2$ alloy and composites exhibited substantial strain rate sensitivity and retain ductility at high strain rates.

Plate-like laminate structures are common and important structural forms in engineering applications such as coatings and micro-devices. Using a facile method of heat treatment, Wei and He[16] synthesized a multilayered sandwich-like structure with each layer composed of large-scale pentagonal dodecahedra of Al-Cu-Fe QCs. Yadav et al.[17] used Al-based single-phase decagonal QC $Al_{66}Co_{17}Cu_{17}$ alloy to extract the corresponding 2D alloy structure. In non-classical theories including nonlocal elasticity theory[18], nonlocal strain gradient theory[19], and modified couple stress theory[20], the nonlocal theory has been widely used in predicting the mechanical properties of nano-materials and nano-structures[21–23] such as nanobeams, graphene nanosheets, and nanoplates. Furthermore, the results based on this theory are in excellent agreement with those obtained from MD simulation and experiments. By establishing the layered plate models, the bending deformation, vibration response, and buckling of 1D and 2D QC layered plates without any elastic medium were analyzed[24–30]. Guo et al.[31] considered the nonlocal buckling of composite nanoplates with coated 1D QCs in an elastic medium. However, to the best of the authors' knowledge, no work on the mechanical behaviors of 2D layered QC plates embedded in an elastic medium has been investigated so far. Therefore, the present study focuses on the vibration and buckling of 2D decagonal QC layered nanoplates on top of or embedded in an elastic medium based on the nonlocal theory.

This paper is organized as follows. In Section 2, we describe the current problem and introduce the basic equations of 2D QCs. In Section 3, we present the vibration and buckling

solutions of the 2D decagonal QC layered nanoplate. According to the quasi-periodic directions, three cases of 2D decagonal QC nanoplates with the elastic medium are considered. Various numerical examples are displayed in Section 4, and the conclusions are drawn in Section 5.

2 Problem description and basic equations

QCs can be quasi-periodic in one, two, or three directions. The 2D QCs considered in this work have a 3D structure in which the atomic arrangement is quasi-periodic in two directions (quasi-periodic plane) and periodic in the other direction perpendicular to the quasi-periodic plane. The horizontal dimensions and total thickness of the N-layered QC nanoplate are L_1, L_2, and H, respectively (see Fig. 1). The vibration and buckling of a 3D rectangular N-layered nanoplate made of 2D decagonal QC and crystal materials are considered in the present study. It is assumed that the four lateral sides of the nanoplate are simply supported, satisfying the following conditions:

$$\begin{cases} u_2 = u_3 = w_2 = \sigma_{11} = H_{11} = 0 \quad \text{at} \quad x_1 = 0 \ \text{ and } \ L_1, \\ u_1 = u_3 = w_1 = \sigma_{22} = H_{22} = 0 \quad \text{at} \quad x_2 = 0 \ \text{ and } \ L_2, \end{cases} \tag{1}$$

where u_i $(i = 1, 2, 3)$ and w_k $(k = 1, 2)$ are the phonon and phason displacements, respectively. σ_{ij} and H_{kj} are the phonon and phason stresses, respectively. Furthermore, the interfaces between different layers are assumed to be perfectly bonded. Namely, the following continuity conditions hold on these interfaces[31]:

$$\boldsymbol{u}^{(m)} = \boldsymbol{u}^{(m+1)}, \quad \boldsymbol{t}_1^{(m)} = \boldsymbol{t}_1^{(m+1)}, \quad m = 1, 2, \cdots, N-1, \tag{2}$$

where $\boldsymbol{u} = (u_1, u_2, u_3, w_1, w_2)^{\mathrm{T}}$ and $\boldsymbol{t}_1 = (\sigma_{13}, \sigma_{23}, \sigma_{33}, H_{13}, H_{23})^{\mathrm{T}}$ are the extended displacement (phonon and phason displacements) and extended out-of-plane stress (phonon and phason stresses) vectors, respectively, in which T denotes the transpose of a matrix or vector.

The 2D decagonal QC layered nanoplate can be located on an elastic medium or embedded in it with the Winkler stiffness k_{W} and the shear modulus k_G, as shown in Fig. 1. For the vibration problem, both the top and bottom surfaces of the QC nanoplate are traction-free. For the buckling problem, the lateral boundary of the QC nanoplate is subjected to the normal compressive stresses of the phonon field along the horizontal x_1- and x_2-directions, i.e., $\bar{\sigma}_{11}$ and $\bar{\sigma}_{22} = \lambda\bar{\sigma}_{11}$, respectively. The nanoplate is under uniaxial compression when $\lambda = 0$ and biaxial compression when $\lambda = 1$.

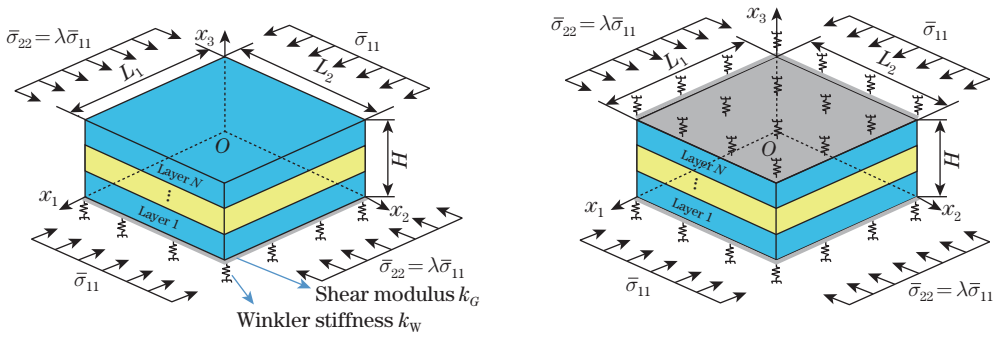

(a) On top of an elastic medium (b) Embedded in an elastic medium

Fig. 1 A 2D decagonal QC N-layered nanoplate on top of an elastic medium and embedded in an elastic medium (color online)

In the linear elasticity theory of QCs, the strain-displacement relations for 2D decagonal QCs are given by

$$\varepsilon_{ij} = \frac{1}{2}(u_{i,j} + u_{j,i}), \quad \omega_{kj} = w_{k,j}, \tag{3}$$

where a comma followed by index i in subscript denotes the partial differentiation with respect to the Cartesian coordinate x_i. ε_{ij} and ω_{ij} are the phonon and phason strains, respectively. The coupled constitutive relations with nonlocal effects in the Cartesian coordinates (x_1, x_2, and x_3) can be written as follows:

$$\begin{cases} (1-l^2\nabla^2)\sigma_{11} = C_{11}\varepsilon_{11} + C_{12}\varepsilon_{22} + C_{13}\varepsilon_{33} + R_1\omega_{11} + R_1\omega_{22}, \\ (1-l^2\nabla^2)\sigma_{22} = C_{12}\varepsilon_{11} + C_{11}\varepsilon_{22} + C_{13}\varepsilon_{33} - R_1\omega_{11} - R_1\omega_{22}, \\ (1-l^2\nabla^2)\sigma_{33} = C_{13}\varepsilon_{11} + C_{13}\varepsilon_{22} + C_{33}\varepsilon_{33}, \quad (1-l^2\nabla^2)\sigma_{31} = 2C_{44}\varepsilon_{13}, \\ (1-l^2\nabla^2)\sigma_{12} = 2C_{66}\varepsilon_{12} - R_1\omega_{12} + R_1\omega_{21}, \quad (1-l^2\nabla^2)\sigma_{23} = 2C_{44}\varepsilon_{23}, \\ (1-l^2\nabla^2)H_{11} = R_1\varepsilon_{11} - R_1\varepsilon_{22} + K_1\omega_{11} + K_2\omega_{22}, \\ (1-l^2\nabla^2)H_{22} = R_1\varepsilon_{11} - R_1\varepsilon_{22} + K_2\omega_{11} + K_1\omega_{22}, \\ (1-l^2\nabla^2)H_{12} = -2R_1\varepsilon_{12} + K_1\omega_{12} - K_2\omega_{21}, \quad (1-l^2\nabla^2)H_{23} = K_4\omega_{23}, \\ (1-l^2\nabla^2)H_{21} = 2R_1\varepsilon_{12} - K_2\omega_{12} + K_1\omega_{21}, \quad (1-l^2\nabla^2)H_{13} = K_4\omega_{13}, \end{cases} \tag{4}$$

where $C_{66} = (C_{11} - C_{12})/2$. $l = e_0 a$ is the nonlocal length with e_0 being a constant appropriate to each material and a being an internal characteristic length (e.g., lattice parameter and granular distance). ∇^2 is the 3D Laplacian operator. C_{ij}, K_i, and R_1 are the phonon elastic modulus, the phason elastic modulus, and the phonon-phason coupling elastic modulus, respectively. For a homogenous and isotropic solid, the nonlocal parameter l would be the same in the constitutive equations as presented in the nonlocal theory by Eringen[32]. However, for anisotropic and multilayered nanoplates made up of different materials, l may be different in different directions and different layers. For simple mathematical computation, the nonlocal parameter l is assumed to be the same in different directions and different layers in this work. The effects of the nonlocal parameter l in different directions on the mechanical behavior of anisotropic materials will be considered in the future study. The effects of the nonlocal parameter in different layers on the bending deformation and buckling of the sandwich nanoplates were previously studied[29,31]. It was observed that different l in different layers only had a slight effect on the bending deformation[29] and critical loads[31] of the multilayered plates.

The equilibrium equations can be expressed as

$$\sigma_{ij,j} = f_i, \quad H_{kj,j} = 0, \tag{5}$$

where $f_i = \rho u_{i,\mathrm{tt}}$ for the vibration problem, and $f_i = \bar{\sigma}_{11}u_{i,11} + \bar{\sigma}_{22}u_{i,22}$ for the buckling problem, in which ρ is the density and the subscript t denotes time.

3 General solutions

In this section, we consider three cases of a 2D decagonal QC layered nanoplate according to its quasi-periodic directions. In Case 1, the x_1-x_2 plane is the quasi-periodic plane, and the x_3-axis is the periodic direction. In Case 2, the x_2-x_3 plane is the quasi-periodic plane, and the x_1-axis is the periodic direction. In Case 3, the x_1-x_3 plane is the quasi-periodic plane, and the x_2-axis is the periodic direction.

Since the treatment for the three cases is similar, we only present the details for Case 1 below. The relevant formulae for Cases 2 and 3 can be found in Ref. [33]. Applying the simply-supported boundary conditions, the general solution of the extended displacement for Case 1 can be assumed as follows:

$$\boldsymbol{u} = \mathrm{e}^{\phi} \begin{pmatrix} a_1 \cos(\alpha x_1) \sin(\beta x_2) \\ a_2 \sin(\alpha x_1) \cos(\beta x_2) \\ a_3 \sin(\alpha x_1) \sin(\beta x_2) \\ a_4 \cos(\alpha x_1) \sin(\beta x_2) \\ a_5 \sin(\alpha x_1) \cos(\beta x_2) \end{pmatrix}, \quad \alpha = m\pi/L_1, \quad \beta = n\pi/L_2, \tag{6}$$

where the coefficients a_i $(i = 1, 2, \cdots, 5)$ are unknown constants (eigenvector components) to be determined. m and n are two positive integers. For vibration, $\phi = sx_3 + \mathrm{i}\omega t$, while for buckling, $\phi = sx_3$, in which s and ω are the eigenvalue and the angular frequency, respectively. It is noted that the normal i denotes the imaginary number ($\mathrm{i}^2 = -1$), whilst the italic i is an index. Then, we can assume the extended out-of-plane stress vector and the extended in-plane stress vector as follows:

$$\boldsymbol{t}_1 = \mathrm{e}^{\phi} \begin{pmatrix} b_1 \cos(\alpha x_1) \sin(\beta x_2) \\ b_2 \sin(\alpha x_1) \cos(\beta x_2) \\ b_3 \sin(\alpha x_1) \sin(\beta x_2) \\ b_4 \cos(\alpha x_1) \sin(\beta x_2) \\ b_5 \sin(\alpha x_1) \cos(\beta x_2) \end{pmatrix}, \quad \boldsymbol{t}_2 = \begin{pmatrix} \sigma_{11} \\ \sigma_{12} \\ \sigma_{22} \\ H_{11} \\ H_{22} \\ H_{12} \\ H_{21} \end{pmatrix} = \mathrm{e}^{\phi} \begin{pmatrix} c_1 \sin(\alpha x_1) \sin(\beta x_2) \\ c_2 \cos(\alpha x_1) \cos(\beta x_2) \\ c_3 \sin(\alpha x_1) \sin(\beta x_2) \\ c_4 \sin(\alpha x_1) \sin(\beta x_2) \\ c_5 \sin(\alpha x_1) \sin(\beta x_2) \\ c_6 \cos(\alpha x_1) \cos(\beta x_2) \\ c_7 \cos(\alpha x_1) \cos(\beta x_2) \end{pmatrix}, \tag{7}$$

where the coefficients b_i $(i = 1, 2, \cdots, 5)$ and c_i $(i = 1, 2, \cdots, 7)$ can be expressed in terms of a_i $(i = 1, 2, \cdots, 5)$ as shown below.

Substitute Eq. (6) into Eqs. (3) and (4). Then, the relation between the vectors $\boldsymbol{a} = (a_1, a_2, a_3, a_4, a_5)^{\mathrm{T}}$ and $\boldsymbol{b} = (b_1, b_2, b_3, b_4, b_5)^{\mathrm{T}}$ can be obtained as follows:

$$(1 - l^2(s^2 - \alpha^2 - \beta^2))\boldsymbol{b} = (-\boldsymbol{R}^{\mathrm{T}} + s\boldsymbol{T})\boldsymbol{a}, \tag{8}$$

where

$$\boldsymbol{R} = \begin{pmatrix} 0 & 0 & C_{13}\alpha & 0 & 0 \\ 0 & 0 & C_{13}\beta & 0 & 0 \\ -C_{44}\alpha & -C_{44}\beta & 0 & 0 & 0 \\ 0 & 0 & 0 & 0 & 0 \\ 0 & 0 & 0 & 0 & 0 \end{pmatrix}, \quad \boldsymbol{T} = \begin{pmatrix} C_{44} & 0 & 0 & 0 & 0 \\ 0 & C_{44} & 0 & 0 & 0 \\ 0 & 0 & C_{33} & 0 & 0 \\ 0 & 0 & 0 & K_4 & 0 \\ 0 & 0 & 0 & 0 & K_4 \end{pmatrix}. \tag{9}$$

Meanwhile, the relation between the vectors $\boldsymbol{a}$ and $\boldsymbol{c} = (c_1, c_2, c_3, c_4, c_5, c_6, c_7)^{\mathrm{T}}$ is

$$(1 - l^2(s^2 - \alpha^2 - \beta^2))\boldsymbol{c} = \begin{pmatrix} -C_{11}\alpha & -C_{12}\beta & C_{13}s & -R_1\alpha & -R_1\beta \\ C_{66}\beta & C_{66}\alpha & 0 & -R_1\beta & R_1\alpha \\ -C_{12}\alpha & -C_{11}\beta & C_{13}s & R_1\alpha & R_1\beta \\ -R_1\alpha & R_1\beta & 0 & -K_1\alpha & -K_2\beta \\ -R_1\alpha & R_1\beta & 0 & -K_2\alpha & -K_1\beta \\ -R_1\beta & -R_1\alpha & 0 & K_1\beta & -K_2\alpha \\ R_1\beta & R_1\alpha & 0 & -K_2\beta & K_1\alpha \end{pmatrix} \boldsymbol{a}. \tag{10}$$

Substituting Eqs. (6) and (7) into Eq. (5) yields

$$\begin{cases} sb_1 = -\alpha c_1 + \beta c_2 - \psi a_1, \quad sb_2 = \alpha c_2 - \beta c_3 - \psi a_2, \quad sb_3 = \alpha b_1 + \beta b_2 - \psi a_3, \\ sb_4 = -\alpha c_4 + \beta c_6, \quad sb_5 = -\beta c_5 + \alpha c_7, \end{cases} \tag{11}$$

where $\psi = \omega^2\rho$ for vibration, and $\psi = \alpha^2\bar{\sigma}_{11} + \beta^2\bar{\sigma}_{22}$ for buckling. Substituting Eqs. (8) and (10) into the right-hand side of Eq. (11), we further have

$$(1 - l^2(s^2 - \alpha^2 - \beta^2))s\boldsymbol{b} = (\boldsymbol{Q} - s\boldsymbol{R} + s^2\boldsymbol{P})\boldsymbol{a}, \tag{12}$$

where

$$\boldsymbol{Q} = \begin{pmatrix} Q_{11} & \alpha\beta(C_{12}+C_{66}) & 0 & R_1(\alpha^2-\beta^2) & 2R_1\alpha\beta \\ \alpha\beta(C_{12}+C_{66}) & Q_{22} & 0 & -2R_1\alpha\beta & R_1(\alpha^2-\beta^2) \\ 0 & 0 & Q_{33} & 0 & 0 \\ R_1(\alpha^2-\beta^2) & -2R_1\alpha\beta & 0 & K_1(\alpha^2+\beta^2) & 0 \\ 2R_1\alpha\beta & R_1(\alpha^2-\beta^2) & 0 & 0 & K_1(\alpha^2+\beta^2) \end{pmatrix}, \tag{13}$$

$$\boldsymbol{P} = l^2\psi \begin{pmatrix} 1 & 0 & 0 & 0 & 0 \\ 0 & 1 & 0 & 0 & 0 \\ 0 & 0 & 1 & 0 & 0 \\ 0 & 0 & 0 & 0 & 0 \\ 0 & 0 & 0 & 0 & 0 \end{pmatrix}, \quad \begin{aligned} Q_{11} &= C_{11}\alpha^2 + C_{66}\beta^2 - (1 + l^2\alpha^2 + l^2\beta^2)\psi, \\ Q_{22} &= C_{66}\alpha^2 + C_{11}\beta^2 - (1 + l^2\alpha^2 + l^2\beta^2)\psi, \\ Q_{33} &= C_{44}\alpha^2 + C_{44}\beta^2 - (1 + l^2\alpha^2 + l^2\beta^2)\psi. \end{aligned} \tag{14}$$

Let $\boldsymbol{d} = s\boldsymbol{a}$. Then, the linear eigensystem can be established as follows:

$$s\begin{pmatrix} \boldsymbol{a} \\ \boldsymbol{d} \end{pmatrix} = \begin{pmatrix} \boldsymbol{0} & \boldsymbol{I} \\ (\boldsymbol{T}-\boldsymbol{P})^{-1}\boldsymbol{Q} & (\boldsymbol{T}-\boldsymbol{P})^{-1}(\boldsymbol{R}^{\mathrm{T}} - \boldsymbol{R}) \end{pmatrix} \begin{pmatrix} \boldsymbol{a} \\ \boldsymbol{d} \end{pmatrix}. \tag{15}$$

The eigenvalues s and eigenvectors $\boldsymbol{a}$ and $\boldsymbol{d}$ are obtained by solving Eq. (15). Then, the vector $\boldsymbol{b}$ can be obtained from Eq. (8). Thus, the general solution for the extended displacement and traction vectors can be expressed as follows:

$$\begin{pmatrix} \boldsymbol{u}(x_3) \\ \boldsymbol{t}_1(x_3) \end{pmatrix} = \begin{pmatrix} \boldsymbol{A}_1 & \boldsymbol{A}_2 \\ \boldsymbol{B}_1 & \boldsymbol{B}_2 \end{pmatrix} \langle \mathrm{e}^{s^* x_3} \rangle \begin{pmatrix} \boldsymbol{k}_1 \\ \boldsymbol{k}_2 \end{pmatrix}, \tag{16}$$

where $\boldsymbol{k}_1$ and $\boldsymbol{k}_2$ are two 5×1 constant vectors to be determined, and

$$\begin{cases} \boldsymbol{A}_1 = (\boldsymbol{a}_1, \quad \boldsymbol{a}_2, \quad \boldsymbol{a}_3, \quad \boldsymbol{a}_4, \quad \boldsymbol{a}_5), \quad \boldsymbol{A}_2 = (\boldsymbol{a}_6, \quad \boldsymbol{a}_7, \quad \boldsymbol{a}_8, \quad \boldsymbol{a}_9, \quad \boldsymbol{a}_{10}), \\ \langle \mathrm{e}^{s^* x_3} \rangle = \mathrm{diag}(\mathrm{e}^{s_1 x_3}, \ \mathrm{e}^{s_2 x_3}, \ \cdots, \mathrm{e}^{s_{10} x_3}), \\ \boldsymbol{B}_1 = (\boldsymbol{b}_1, \quad \boldsymbol{b}_2, \quad \boldsymbol{b}_3, \quad \boldsymbol{b}_4, \quad \boldsymbol{b}_5), \quad \boldsymbol{B}_2 = (\boldsymbol{b}_6, \quad \boldsymbol{b}_7, \quad \boldsymbol{b}_8, \quad \boldsymbol{b}_9, \quad \boldsymbol{b}_{10}). \end{cases} \tag{17}$$

If the extended stress and displacement vectors of the bottom layer of the nanoplate are used to determine $\boldsymbol{k}_1$ and $\boldsymbol{k}_2$, the propagating relations of the solutions at any x_3-level and at the bottom interface of a given layer can be obtained from Eq. (16) as follows:

$$\begin{pmatrix} \boldsymbol{u}(x_3) \\ \boldsymbol{t}_1(x_3) \end{pmatrix} = \begin{pmatrix} \boldsymbol{A}_1 & \boldsymbol{A}_2 \\ \boldsymbol{B}_1 & \boldsymbol{B}_2 \end{pmatrix} \langle \mathrm{e}^{s^* x_3} \rangle \begin{pmatrix} \boldsymbol{A}_1 & \boldsymbol{A}_2 \\ \boldsymbol{B}_1 & \boldsymbol{B}_2 \end{pmatrix}^{-1} \begin{pmatrix} \boldsymbol{u}(0) \\ \boldsymbol{t}_1(0) \end{pmatrix} = \boldsymbol{M}(x_3) \begin{pmatrix} \boldsymbol{u}(0) \\ \boldsymbol{t}_1(0) \end{pmatrix}. \tag{18}$$

For the layered QC nanoplate, we can find the following relations between the extended displacement and the extended stress vectors on the bottom surface $x_3 = 0$ and the top surface $x_3 = H$ by utilizing the continuity condition (2):

$$\begin{pmatrix} \boldsymbol{u}(H) \\ \boldsymbol{t}_1(H) \end{pmatrix} = \boldsymbol{M}(h_N)\boldsymbol{M}(h_{N-1})\cdots\boldsymbol{M}(h_2)\boldsymbol{M}(h_1)\begin{pmatrix} \boldsymbol{u}(0) \\ \boldsymbol{t}_1(0) \end{pmatrix} = \boldsymbol{J}\begin{pmatrix} \boldsymbol{u}(0) \\ \boldsymbol{t}_1(0) \end{pmatrix}. \tag{19}$$

3.1 A 2D decagonal QC layered nanoplate without an elastic medium

If there is no elastic medium surrounding the 2D decagonal QC layered nanoplate and the top and bottom surfaces of the nanoplate are traction-free, Eq. (19) becomes

$$\begin{pmatrix} \boldsymbol{u}(H) \\ \boldsymbol{0} \end{pmatrix} = \begin{pmatrix} \boldsymbol{J}_{11} & \boldsymbol{J}_{12} \\ \boldsymbol{J}_{21} & \boldsymbol{J}_{22} \end{pmatrix}\begin{pmatrix} \boldsymbol{u}(0) \\ \boldsymbol{0} \end{pmatrix}, \tag{20}$$

where $\boldsymbol{J}_{ij}$ $(i, j = 1, 2)$ are the submatrices of $\boldsymbol{J}$ in Eq. (19). Let the determinant of $\boldsymbol{J}_{21}$ be 0. Then, we can determine the frequency or critical buckling load of the 2D decagonal QC layered nanoplate.

3.2 A 2D decagonal QC layered nanoplate on top of an elastic medium

We consider a 2D decagonal QC layered nanoplate on top of an elastic medium. The interaction between the QC nanoplate and the elastic medium is assumed to be the Pasternak-type foundation[34]. Thus, the traction boundary conditions are

$$\boldsymbol{t}_1(H) = (0,\ 0,\ 0,\ 0,\ 0)^{\mathrm{T}}, \quad \boldsymbol{t}_1(0) = (0,\ 0,\ q_3^0,\ 0,\ 0)^{\mathrm{T}}, \tag{21}$$

where

$$q_3^0 = k_{\mathrm{W}}(u_3^0) - k_G((u_3^0)_{,11} + (u_3^0)_{,22}), \tag{22}$$

in which u_3^0 denotes the deflection on the bottom surface of the nanoplate. Substituting Eq. (21) into Eq. (19) and expanding it, we obtain

$$\boldsymbol{u}(0) = (0,\ 0,\ u_3^0,\ 0,\ 0)^{\mathrm{T}} = -\boldsymbol{J}_{21}^{-1}\boldsymbol{J}_{22}\boldsymbol{t}_1(0). \tag{23}$$

From Eqs. (21)–(23), the frequency or critical buckling load can be solved by

$$1 - X_{33}(k_{\mathrm{W}} + k_G(\alpha^2 + \beta^2)) = 0, \tag{24}$$

where X_{33} is the element (3,3) of $-\boldsymbol{J}_{21}^{-1}\boldsymbol{J}_{22}$.

3.3 A 2D decagonal QC layered nanoplate embedded in an elastic medium

If the 2D decagonal QC nanoplate is embedded in an elastic medium, the traction boundary conditions are given by

$$\boldsymbol{t}_1(H) = (0,\ 0,\ q_3^H,\ 0,\ 0)^{\mathrm{T}}, \quad \boldsymbol{t}_1(0) = (0,\ 0,\ q_3^0,\ 0,\ 0)^{\mathrm{T}}, \tag{25}$$

where

$$q_3^H = -k_{\mathrm{W}}(u_3^H) + k_G((u_3^H)_{,11} + (u_3^H)_{,22}), \quad q_3^0 = k_{\mathrm{W}}(u_3^0) - k_G((u_3^0)_{,11} + (u_3^0)_{,22}), \tag{26}$$

in which u_3^H denotes the deflection on the top of the nanoplate. Substituting Eq. (25) into Eq. (19) yields

$$\begin{cases} \boldsymbol{u}(0) = (0,\ 0,\ u_3^0,\ 0,\ 0)^{\mathrm{T}} = \boldsymbol{J}_{21}^{-1}(\boldsymbol{t}_1(H) - \boldsymbol{J}_{22}\boldsymbol{t}_1(0)), \\ \boldsymbol{u}(H) = (0,\ 0,\ u_3^H,\ 0,\ 0)^{\mathrm{T}} = \boldsymbol{J}_{11}\boldsymbol{J}_{21}^{-1}\boldsymbol{t}_1(H) + (\boldsymbol{J}_{12} - \boldsymbol{J}_{11}\boldsymbol{J}_{21}^{-1}\boldsymbol{J}_{22})\boldsymbol{t}_1(0). \end{cases} \tag{27}$$

With Eqs. (25)–(27), the vibration frequency or critical buckling load can be solved from the following equation:

$$(1+B_{33}(k_{\mathrm{W}}+k_G(\alpha^2+\beta^2)))(1+C_{33}(k_{\mathrm{W}}+k_G(\alpha^2+\beta^2)))$$
$$+A_{33}D_{33}(k_{\mathrm{W}}+k_G(\alpha^2+\beta^2))^2=0, \tag{28}$$

where A_{33}, B_{33}, C_{33}, and D_{33} are the elements (3,3) of $\boldsymbol{J}_{21}^{-1}$, $\boldsymbol{J}_{21}^{-1}\boldsymbol{J}_{22}$, $\boldsymbol{J}_{11}\boldsymbol{J}_{21}^{-1}$, and $\boldsymbol{J}_{12}-\boldsymbol{J}_{11}\boldsymbol{J}_{21}^{-1}\boldsymbol{J}_{22}$, respectively.

4 Numerical examples

In this section, we analyze the nonlocal vibration and buckling of 2D decagonal QC homogeneous nanoplates and two sandwich nanoplates made of 2D decagonal Al-Ni-Co QC and $BaTiO_3$ crystal with the elastic medium for mode $(m,n)=(1,1)$. The effects of the quasiperiodic direction, length-to-width ratio, thickness of nanoplate, nonlocal parameter, stacking sequence, and elastic medium on the vibration frequency and critical buckling load are analyzed. The material properties for the 2D decagonal Al-Ni-Co QC and $BaTiO_3$ crystal are listed in Table 1. It should be pointed out that the piezoelectric coupling must be considered in piezoelectric QC (PQC) materials[29]. In this section, QC and C denote, respectively, Al-Ni-Co QC and $BaTiO_3$ crystal.

Table 1 Material properties of 2D Al-Ni-Co QC (denoted as QC)[35] and $BaTiO_3$ crystal (denoted as C)[36] (C_{ij}, K_i, and R_1 in $10^9\,\mathrm{N/m^2}$ and ρ in $10^3\,\mathrm{kg/m^3}$)

Material	$C_{11}=C_{22}$	C_{12}	$C_{13}=C_{23}$	C_{33}	$C_{44}=C_{55}$	C_{66}
QC	234.33	57.41	66.63	232.21	70.19	88.46
C	166	77	78	162	43	44.5
Material	K_1	K_2	K_4	R_1	ρ	
QC	122	24	12	8.846	4.186	
C	–	–	–	–	5.8	

4.1 Vibration

To verify the accuracy of the present 3D model, we first apply our solution to thin graphene sheets and compare our results with those based on the reformulated sinusoidal shear deformation plate theory[37]. This sheet is on the top of an elastic medium (with given normalized k_1 and k_2 below), and its material properties and geometric parameters are taken from Ref. [37] as $E=1\,\mathrm{TPa}$, Poisson's ratio $\nu=0.19$, mass density $\rho=2\,300\,\mathrm{kg/m^3}$, $H=0.34\,\mathrm{nm}$, and $L_1/H=L_2/H=10$. The following dimensionless parameters are used in the comparison:

$$\overline{\omega}=\frac{\omega(L_1)^2}{\pi^2}\sqrt{\frac{\rho h}{D}},\quad k_1=\frac{k_{\mathrm{W}}D}{(L_1)^4},\quad k_2=\frac{k_GD}{(L_1)^2},\quad D=\frac{H^3E}{12(1-\nu^2)}. \tag{29}$$

Table 2 lists the dimensionless fundamental frequencies of the single graphene sheet predicted by the present 3D solution as compared with the existing results. It is observed that these frequencies agree well with those based on the reformulated sinusoidal shear deformation plate theory[37]. This partially verifies our 3D solution. We now analyze the vibration response of a homogeneous 2D decagonal QC nanoplate and two sandwich nanoplates made of 2D decagonal QCs and crystals by using the present 3D solution. In the analysis, the following dimensionless parameters are used:

$$\Omega=\omega L_2\sqrt{\frac{\rho}{C_{\max}}},\quad K_{\mathrm{W}}=\frac{k_{\mathrm{W}}L_2}{C_{\max}},\quad K_G=\frac{k_G}{L_2C_{\max}}, \tag{30}$$

where $C_{\max}$ denotes the maximum elastic modulus of the nanoplates.

Table 2 Dimensionless fundamental frequencies $\overline{\omega}$ of a thin graphene sheet by the present solution, as compared with those by Sobhy[37] (l^2 in nm^2)

l^2	$k_1=100,\ k_2=0$		$k_1=0,\ k_2=20$		$k_1=100,\ k_2=20$	
	Ref. [37]	Present	Ref. [37]	Present	Ref. [37]	Present
0	2.183 96	2.182 99	2.784 10	2.778 51	2.960 17	2.953 19
1	1.549 03	1.506 70	2.319 69	2.299 97	2.528 31	2.511 96
2	1.364 79	1.334 34	2.200 92	2.192 49	2.419 79	2.413 78
3	1.274 85	1.251 77	2.146 29	2.132 67	2.370 20	2.367 70
4	1.221 22	1.203 54	2.114 86	2.113 40	2.341 77	2.339 88

Table 3 shows the dimensionless fundamental frequencies of a homogeneous 2D decagonal QC nanoplate on top of the elastic medium or embedded in it, for $L_1/L_2 = 0.5, 1$, and 1.5 with fixed $L_2 = 100\,\text{nm}$. The nonlocal parameter l reveals the small-scale effect on the responses of nano-structures. Generally, for the analysis of carbon nanotubes, the nonlocal parameters are taken in the range from 0 nm to 2 nm[38]. The critical buckling loads in a simply supported square monolayer graphene sheet derived by Ansari and Rouhi[39] were in excellent agreement with their MD simulations and the solutions by the differential quadrature method[40] for $l = 0 - 2\,\text{nm}$. Thus, we take an acceptable value $l = 2\,\text{nm}$ ($l/L_2 = 0.02$) in the present analysis. Notice that in our previous work[41], we found that the variation of the magnetic potential when $l/H > 0.06$ displayed an opposite trend to that when $l/H < 0.06$. Li et al.[42] adopted a dimensionless nonlocal parameter, and determined the upper limit of the scale parameter from the nano-structural dependence of the nonlocal dynamic behavior, obeying the nonlocal softening mechanism. A crack length or wave length was used by Eringen[43] to determine a dimensionless nonlocal parameter. For the vibration response and buckling behavior analyzed here, the length or width of the nanoplate is used as the external characteristic length scale to normalize the nonlocal parameter, i.e., l/L_2. It is observed that the dimensionless frequencies of the 2D decagonal QC nanoplate always decrease with increasing L_1/L_2. It is interesting to note that when $L_1/L_2 = 1$, Case 1 has the highest frequency, and the frequency of Case 2 is almost the same as that of Case 3. Furthermore, Case 2 has the highest frequency when $L_1/L_2 > 1$, and Case 3 has the highest frequency when $L_1/L_2 < 1$, which is attributed to the quasiperiodic structure and geometrical size. Both the Winkler stiffness K_W and the shear modulus K_G of the elastic medium can help increase the eigen frequency of a 2D decagonal QC nanoplate.

Table 3 Dimensionless fundamental frequencies Ω of the 2D decagonal QC nanoplate with an elastic medium

K_W	K_G	L_1/L_2	On top of the elastic medium			Embedded in the elastic medium		
			Case 1	Case 2	Case 3	Case 1	Case 2	Case 3
0.05	0	0.5	2.600 3	2.596 0	2.692 8	2.627 5	2.623 1	2.718 8
		1	1.335 3	1.329 8	1.329 8	1.389 7	1.384 1	1.384 1
		1.5	1.050 1	1.051 7	1.038 0	1.119 7	1.121 0	1.108 2
0	0.001	0.5	2.599 9	2.595 6	2.692 5	2.626 8	2.622 3	2.718 1
		1	1.301 5	1.296 1	1.296 1	1.323 8	1.318 3	1.318 3
		1.5	0.977 8	0.999 6	0.985 2	1.019 1	1.020 9	1.006 7
0.05	0.001	0.5	2.626 7	2.622 2	2.718 0	2.680 1	2.675 2	2.768 7
		1	1.356 7	1.351 2	1.351 2	1.430 9	1.425 2	1.425 2
		1.5	1.070 2	1.071 6	1.058 2	1.157 2	1.158 3	1.146 0

Table 4 shows the dimensionless fundamental frequencies of two sandwich QC/C/QC and C/QC/C nanoplates (Case 1) for $L_1/L_2 = 0.05$, 1, and 1.5, where $L_2 = 100\,\text{nm}$, $H/L_2 = 0.3$, $K_\text{W} = 0.05$, and $K_G = 1 \times 10^{-3}$. It can be observed that both the nonlocal parameter and the length-to-width ratio can lead to a decrease in the eigen frequencies. Similar to the homogeneous

Table 4 Dimensionless fundamental frequencies Ω of the sandwich QC/C/QC and C/QC/C nanoplates

l/L_2	L_1/L_2	Without an elastic medium		On top of the elastic medium		Embedded in the elastic medium	
		QC/C/QC	C/QC/C	QC/C/QC	C/QC/C	QC/C/QC	C/QC/C
0	0.5	2.665 6	2.273 2	2.730 8	2.332 2	2.795 6	2.390 4
	1	1.349 1	1.096 4	1.440 8	1.189 0	1.527 8	1.275 7
	1.5	1.036 7	0.829 6	1.146 3	0.943 6	1.247 2	1.046 0
0.02	0.5	2.640 2	2.249 2	2.706 7	2.309 0	2.772 6	2.368 1
	1	1.343 8	1.091 2	1.436 1	1.184 4	1.523 5	1.271 4
	1.5	1.033 7	0.826 7	1.143 8	9.410 7	1.244 9	1.043 8
0.04	0.5	2.569 9	2.182 1	2.638 4	2.244 4	2.705 8	2.305 7
	1	1.328 3	1.075 9	1.422 2	1.170 7	1.511 1	1.259 1
	1.5	1.024 9	0.817 9	1.136 2	9.336 8	1.238 4	1.037 4

nanoplate case, the surrounding elastic medium can help increase the eigen frequencies. The frequencies of the sandwich QC/C/QC nanoplate are much higher than those of the sandwich C/QC/C nanoplate. For these two sandwich nanoplates without an elastic medium, our results are the same as those in Ref. [44].

Figures 2 and 3 show the effects of the normalized shear modulus K_G and the normalized Winkler stiffness K_{W} of the elastic medium on the vibration frequencies of a homogeneous 2D decagonal QC nanoplate for given $L_1 = L_2 = 100\,\mathrm{nm}$ and $H/L_2 = 0.3$. In Fig. 2, $K_{\mathrm{W}} = 0.05$ and $K_G \in [0, 1 \times 10^{-3}]$. In Fig. 3, $K_G = 1 \times 10^{-3}$ and $K_{\mathrm{W}} \in [0, 0.05]$. It is observed that the dimensionless fundamental frequencies always increase with increasing K_G and K_{W}. When the nanoplate is embedded in the elastic medium, its fundamental frequency is higher than the one on top of the elastic medium. Furthermore, Case 1 has the highest frequency, and the frequencies of Case 2 and Case 3 are the same when $L_1 = L_2$.

Figure 4 shows the effects of the nanoplate thickness on the vibration frequencies of the sandwich QC/C/QC and C/QC/C plates (Case 1) for given $L_1 = L_2 = 100\,\mathrm{nm}$, $K_{\mathrm{W}} = 0.05$, and $K_G = 1 \times 10^{-3}$, respectively. It is observed that the dimensionless fundamental frequencies always increase with increasing the nanoplate thickness. The eigen frequency decreases in the order as (from large to small): embedded in the elastic medium, on top of the elastic medium, and without an elastic medium. This indicates that the surrounding elastic medium can effectively enhance the stiffness of the nanoplate. The dimensionless frequency of the sandwich QC/C/QC nanoplate is higher than that of the sandwich C/QC/C nanoplate, indicating that the QC materials are suitable for surface coatings in engineering practice.

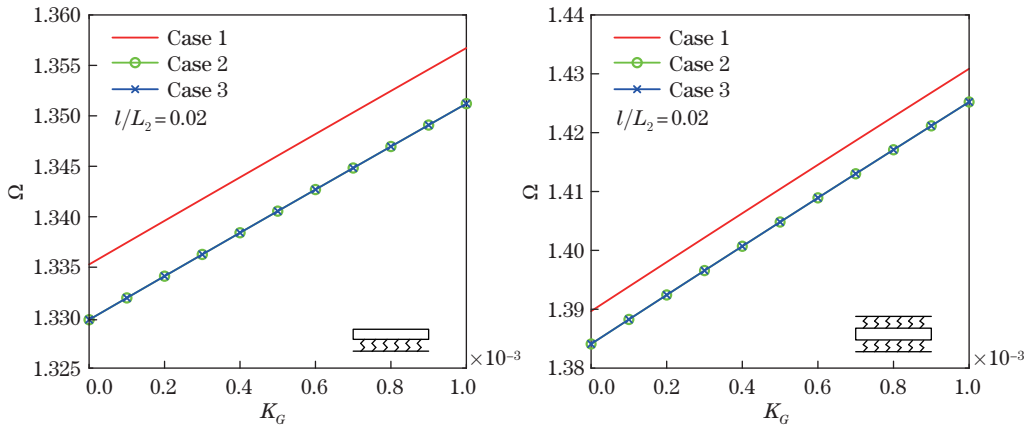

(a) On top of the elastic medium (b) Embedded in the elastic medium

Fig. 2 Variations of the dimensionless fundamental frequencies Ω of the 2D decagonal QC nanoplate with the normalized shear modulus K_G on top of the elastic medium and embedded in the elastic medium (color online)

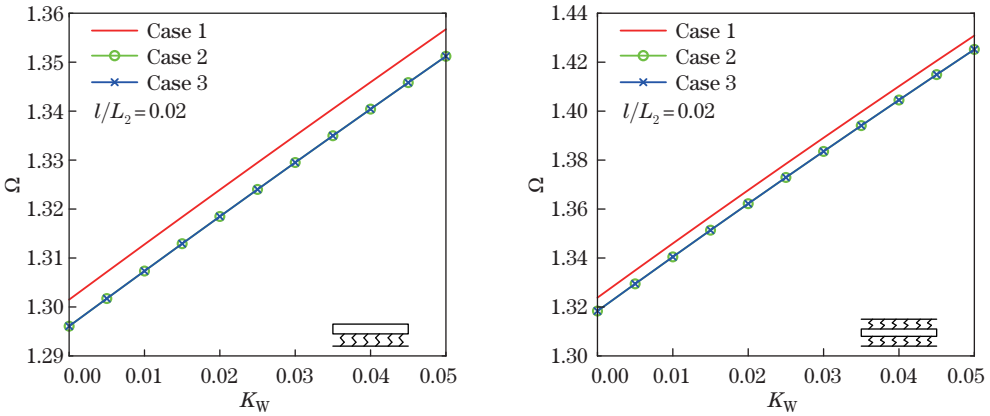

(a) On top of the elastic medium (b) Embedded in the elastic medium

Fig. 3 Variations of the dimensionless fundamental frequencies Ω of the 2D decagonal QC nanoplate with the normalized Winkler stiffness K_W on top of the elastic medium and embedded in the elastic medium (color online)

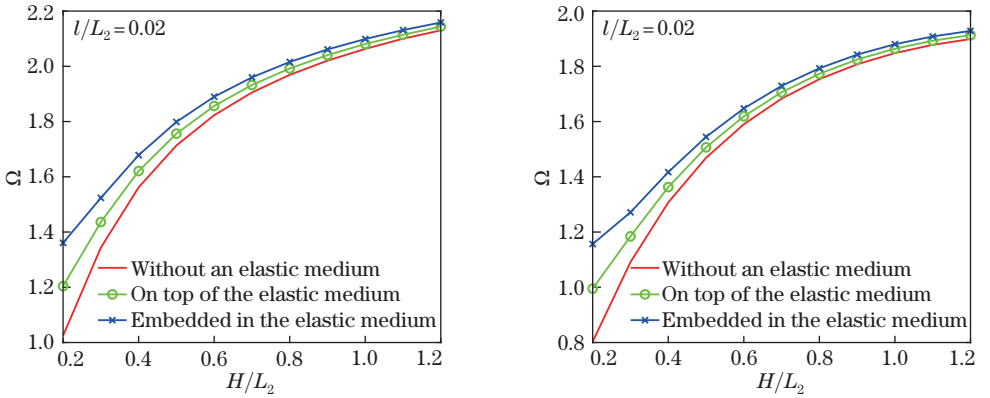

(a) QC/C/QC (b) C/QC/C

Fig. 4 Variations of the dimensionless fundamental frequencies Ω of the sandwich QC/C/QC and C/QC/C nanoplates versus the thickness of the nanoplate (color online)

4.2 Buckling

Sarrami-Foroushani and Azhari[45] used the thin-plate theory to study the nonlocal buckling of single and multi-layered graphene sheets. To verify the correctness of the present 3D solution, the model parameters in Ref. [45] are used here for the graphene: $E = 1.06\,\text{TPa}$, Poisson's ratio $\nu = 0.25$, and the mass density $\rho = 2\,250\,\text{kg/m}^3$. The buckling coefficient in the comparison is defined by $K = (12(\sigma_{11})_{\text{cr}}(1-\nu^2)(L_1/H)^2)(\pi^2 E)^{-1}$.

It can be observed from Table 5 that the buckling coefficient K by the present 3D solution is in good agreement with that by the thin-plate theory[45] when the nanoplate is relatively thin. However, when the nanoplate is thick, the difference between the two becomes large since the thin-plate theory[45] fails to work.

In Subsection 4.1, we compare our solution with the thin-plate theory to verify the accuracy of the present 3D model. Here, we will compare the present results with those of the orthotropic thick plate[46]. The material coefficients of the orthotropic material are shown in Table 6, and the dimensionless critical stress is defined by $k_x = ((\sigma_{11})_{\text{cr}}/C_{11})(12/\pi^2)(L_2/H)^2$. It can be found from Table 7 that the critical buckling coefficient k_x obtained from the present method agrees well with that obtained by the thick-plate theory[46]. Therefore, the present theoretical 3D model can be reduced to both thin plates and medium-thick plates.

Table 5 Buckling coefficient K of a single graphene sheet by the present 3D solution, as compared with those in Ref. [45]

$L_1 = L_2$	$l = 0$ nm		$l = 1$ nm		$l = 1.5$ nm		$l = 2$ nm	
	Ref. [45]	Present	Ref. [45]	Present	Ref. [45]	Present	Ref. [45]	Present
5	4.000 0	3.883 7	2.101 6	1.910 9	1.121 9	1.168 7	0.642 9	0.757 8
10	4.000 0	3.971 6	3.340 6	3.149 9	2.769 9	2.498 4	2.101 6	1.943 2
15	4.000 0	3.989 2	3.677 5	3.572 8	3.600 3	3.156 4	2.961 0	2.723 3
20	4.000 0	3.982 7	3.811 9	3.745 8	3.600 3	3.479 3	3.340 7	3.153 6
30	4.000 0	4.030 8	3.914 2	3.897 6	3.811 9	3.764 3	3.677 5	3.564 5
40	4.000 0	3.967 9	3.951 3	3.967 9	3.892 0	3.849 5	3.812 0	3.731 0
50	4.000 0	3.979 0	3.968 7	3.979 0	3.930 2	3.979 0	3.877 6	3.793 9
100	4.000 0	4.071 5	3.992 2	4.071 5	3.982 3	4.071 5	3.968 8	4.071 5

Table 6 Normalized material properties of an orthotropic material

C_{22}/C_{11}	C_{33}/C_{11}	C_{12}/C_{11}	C_{13}/C_{11}	C_{23}/C_{11}	C_{44}/C_{11}	C_{55}/C_{11}	C_{66}/C_{11}
0.543 10	0.530 17	0.233 19	0.010 78	0.098 28	0.262 93	0.159 91	0.266 81

Table 7 Comparison of the buckling coefficient k_x of the orthotropic rectangular thick plate obtained by the present 3D model with those in Ref. [46]

H/L_2	0.05	0.1	0.2
Ref. [46]	2.966	2.770	2.210
Present	2.959 61	2.770 05	2.209 87

We further consider the buckling behavior of a homogeneous 2D decagonal QC nanoplate and two sandwich nanoplates made of 2D decagonal QCs and crystals based on the present 3D solution. The effects of the length-to-width ratio, plate thickness, nonlocal parameter, stacking sequence, quasiperiodic direction, and elastic medium on the critical buckling loads are analyzed under both uniaxial and biaxial compression. The dimensionless shear modulus K_G and Winkler stiffness K_{W} as defined in Eq. (30) are used. Furthermore, the dimensionless critical buckling load is normalized as $(\bar{\sigma}_{11})_{\mathrm{cr}} = (\sigma_{11})_{\mathrm{cr}}/C_{\max}$.

Table 8 shows the dimensionless critical buckling loads $(\bar{\sigma}_{11})_{\mathrm{cr}}$ of the sandwich QC/C/QC and C/QC/C nanoplates (Case 1) for $L_1/L_2 = 0.05$, 1, and 1.5, where $L_2 = 100$ nm, $H/L_2 = 0.3$, $K_{\mathrm{W}} = 0.05$, and $K_G = 1 \times 10^{-3}$ under uniaxial ($\lambda = 0$) and biaxial ($\lambda = 1$) compression. It can be observed that under both uniaxial and biaxial compression, the dimensionless critical buckling loads of the sandwich QC/C/QC nanoplate are larger than those of the sandwich C/QC/C nanoplate. The surrounding elastic medium always increases the critical buckling loads of the sandwich nanoplate. Furthermore, when L_1/L_2 is large, the dimensionless critical buckling loads under uniaxial compression can be 2–3 times larger than those under biaxial compression.

Figure 5 shows the variations of the dimensionless critical buckling loads of a homogeneous 2D decagonal QC nanoplate with the length-to-width ratio under uniaxial ($\lambda = 0$) and biaxial ($\lambda = 1$) compression for $L_2 = 100$ nm and $H/L_2 = 0.3$. The nonlocal parameter is fixed at $l/L_2 = 0.02$. It can be seen from Fig. 5 that when L_1/L_2 increases, the dimensionless critical buckling loads of the homogeneous QC nanoplate decrease first and then increase under uniaxial compression (see Fig. 5(a)). However, they always decrease under biaxial compression (see Fig. 5(b)). It is interesting to note that the dimensionless critical buckling loads for the three cases of quasiperiodic structures depend on the length-to-width ratio of the QC nanoplate. For example, Case 3 displays the highest critical buckling load when L_1/L_2 is small but the lowest critical buckling load when L_1/L_2 becomes large (see Fig. 5(a)). Under uniaxial compression, the dimensionless critical buckling load reaches its minimum at $L_1/L_2 \approx 0.74$.

Table 8 Dimensionless critical buckling loads $(\bar{\sigma}_{11})_{\rm cr}$ of the sandwich QC/C/QC and C/QC/C nanoplates

l/L_2	λ	L_1/L_2	Without an elastic medium		On top of the elastic medium		Embedded in the elastic medium	
			QC/C/QC	C/QC/C	QC/C/QC	C/QC/C	QC/C/QC	C/QC/C
0	0	0.5	0.146 0	0.119 1	0.153 2	0.125 3	0.160 6	0.131 8
		1	0.149 7	0.108 3	0.170 8	0.130 3	0.191 8	0.150 0
		1.5	0.199 0	0.142 7	0.243 2	0.184 6	0.288 0	0.226 8
	1	0.5	0.116 8	0.095 3	0.122 6	0.100 3	0.128 5	0.105 3
		1	0.074 8	0.055 4	0.085 4	0.065 2	0.096 0	0.075 0
		1.5	0.061 2	0.043 9	0.074 9	0.056 8	0.886 2	0.069 8
0.02	0	0.5	0.143 2	0.116 6	0.150 5	0.122 9	0.158 0	0.129 2
		1	0.148 5	0.109 8	0.169 6	0.129 3	0.190 9	0.149 0
		1.5	0.197 8	0.141 7	0.242 1	0.183 6	0.286 9	0.225 9
	1	0.5	0.114 6	0.093 2	0.120 4	0.098 3	0.126 4	0.103 4
		1	0.074 2	0.054 9	0.084 8	0.064 7	0.954 4	0.074 5
		1.5	0.060 9	0.043 6	0.074 5	0.056 5	0.882 7	0.069 5
0.04	0	0.5	0.135 4	0.109 7	0.142 8	0.116 1	0.150 4	0.122 5
		1	0.145 0	0.106 7	0.166 3	0.126 3	0.187 7	0.146 1
		1.5	0.194 3	0.138 7	0.238 9	0.180 8	0.283 8	0.223 1
	1	0.5	0.108 5	0.087 8	0.114 3	0.092 8	0.120 2	0.098 0
		1	0.072 5	0.053 4	0.083 1	0.063 2	0.093 9	0.073 1
		1.5	0.059 8	0.042 7	0.073 5	0.055 6	0.087 3	0.068 7

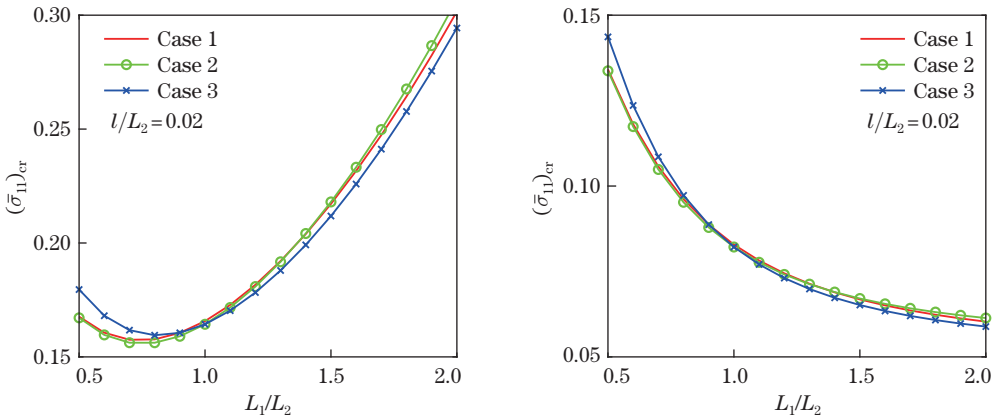

(a) Uniaxial compression (b) Biaxial compression

Fig. 5 Variations of the dimensionless critical buckling load of the 2D decagonal QC nanoplate under uniaxial and biaxial compression without an elastic medium but with a fixed nonlocal parameter (color online)

Figures 6 and 7 show the effects of the normalized shear modulus K_G and normalized Winkler stiffness $K_{\rm W}$ of the elastic medium with fixed $L_2 = 100\,{\rm nm}$, $L_1 = 0.74 \times L_2$, and $H/L_2 = 0.3$. We also fix $K_{\rm W} = 0.05$ and $K_G \in [0, 1 \times 10^{-3}]$ in Fig. 6 and $K_G = 1 \times 10^{-3}$ and $K_{\rm W} \in [0, 0.05]$ in Fig. 7. It can be found that the critical buckling loads always increase with increasing the normalized Winkler stiffness $K_{\rm W}$ and normalized shear modulus K_G. The critical buckling loads of the nanoplate under biaxial compression are smaller than those under uniaxial compression. Furthermore, the elastic medium and quasiperiodic direction can both significantly affect the critical buckling loads of the 2D decagonal QC nanoplate.

The effects of the nanoplate thickness and nonlocal parameter on the dimensionless critical buckling load of sandwich QC/C/QC and C/QC/C nanoplates (Case 1) with $L_2 = 100\,{\rm nm}$, $L_1 = 0.74 \times L_2$, $K_{\rm W} = 0.05$, and $K_G = 1 \times 10^{-3}$ are shown in Fig. 8. It is observed that, under both uniaxial and biaxial compression, the critical buckling loads of both sandwich nanoplates

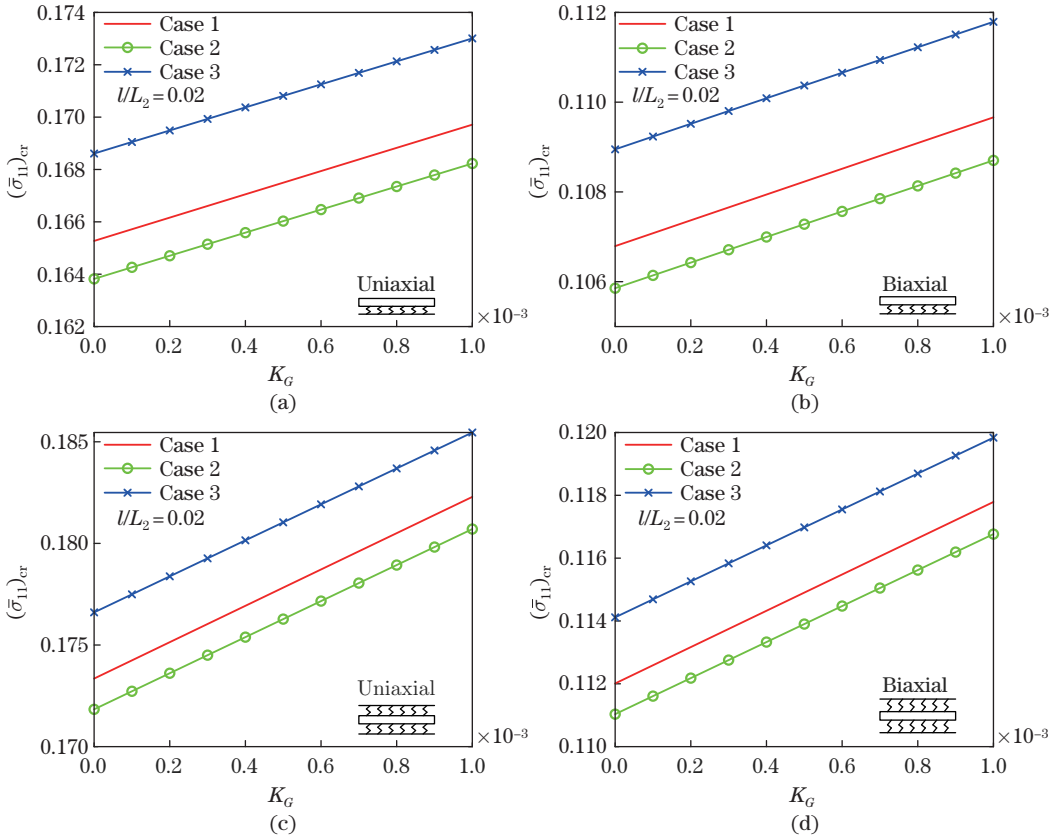

Fig. 6 Variations of the dimensionless critical buckling load of the plate versus the normalized shear modulus K_G (with a fixed nonlocal parameter) under (a) uniaxial compression with the plate on top of the elastic medium; (b) biaxial compression with the plate on top of the elastic medium; (c) uniaxial compression with the plate embedded in the elastic medium; (d) biaxial compression with the plate embedded in the elastic medium (color online)

increase with increasing the nanoplate thickness. The critical buckling loads of the two embedded sandwich nanoplates are larger than those on the elastic medium or those without the elastic medium support. Besides, the critical buckling loads of the sandwich QC/C/QC nanoplate are larger than those of the sandwich C/QC/C nanoplate.

5 Conclusions

Based on the nonlocal theory, the vibration and buckling behaviors of the 2D decagonal QC layered nanoplate with an elastic medium are investigated. The analytical solutions of the vibration frequency and critical buckling load of the nanoplate in the elastic medium are obtained by solving the eigensystem and using the propagator matrix method. Numerical examples are illustrated to show the effects of the quasiperiodic direction, length-to-width ratio, thickness of the nanoplate, nonlocal parameter, stacking sequence, and elastic medium on the vibration frequency and the critical buckling load. The following conclusions can be drawn from the numerical results.

(i) The present exact 3D model can correctly predict the vibration and buckling behaviors of 2D decagonal QC layered nanoplates along the thickness direction rather than the previous thin plate and medium-thick plate. The nature frequencies and critical buckling loads of the 2D decagonal QC nanoplate always increase with increasing the nanoplate thickness.

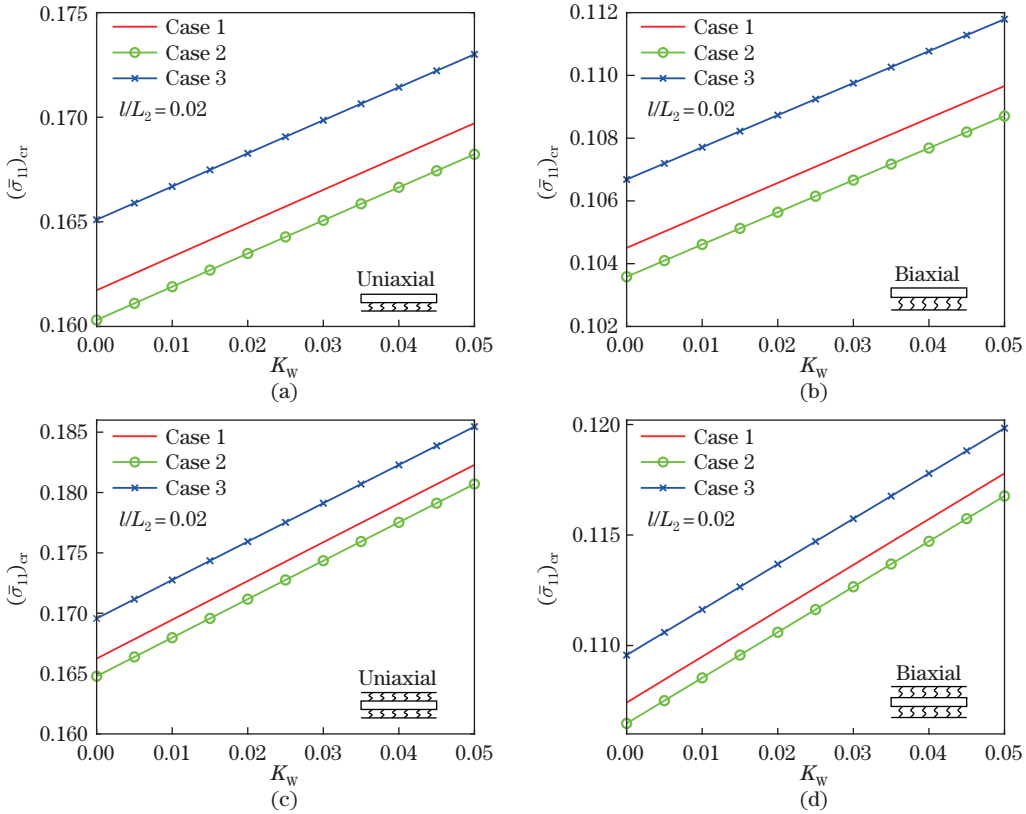

Fig. 7 Variations of the dimensionless critical buckling load of the plate versus the normalized Winkler stiffness K_W (with a fixed nonlocal parameter) under (a) uniaxial compression with the plate on top of the elastic medium; (b) biaxial compression with the plate on top of the elastic medium; (c) uniaxial compression with the plate embedded in the elastic medium; (d) biaxial compression with the plate embedded in the elastic medium (color online)

(ii) The Winkler stiffness k_W and shear modulus k_G of the surrounding elastic medium can help increase the vibration frequency and critical buckling load of the 2D decagonal QC nanoplate. Furthermore, the size-dependent vibration frequency and critical buckling load can be reduced to the classical results at macro-scale when the nonlocal parameter is neglected.

(iii) With increasing the length-to-width ratio of the nanoplate, the vibration frequencies and critical buckling loads under biaxial compression always decrease. Under uniaxial compression, on the other hand, the critical buckling load varies differently, having a minimum at $L_1/L_2 \approx 0.74$.

(iv) The quasiperiodic direction of the 2D decagonal QC structure has a great effect on the vibration frequency and critical bucking load. When $L_1/L_2 = 1$, the vibration frequency and the critical bucking load for Case 1 reach their maxima. When $L_1/L_2 > 1$, the vibration frequency and critical bucking load for Case 2 reach their maxima. When $L_1/L_2 < 1$, the vibration frequency and critical bucking load for Case 3 reach their maxima.

(v) The vibration frequencies and critical buckling loads of the sandwich QC/C/QC nanoplate are larger than those of the sandwich C/QC/C nanoplate, indicating that QCs are suitable as coating materials.

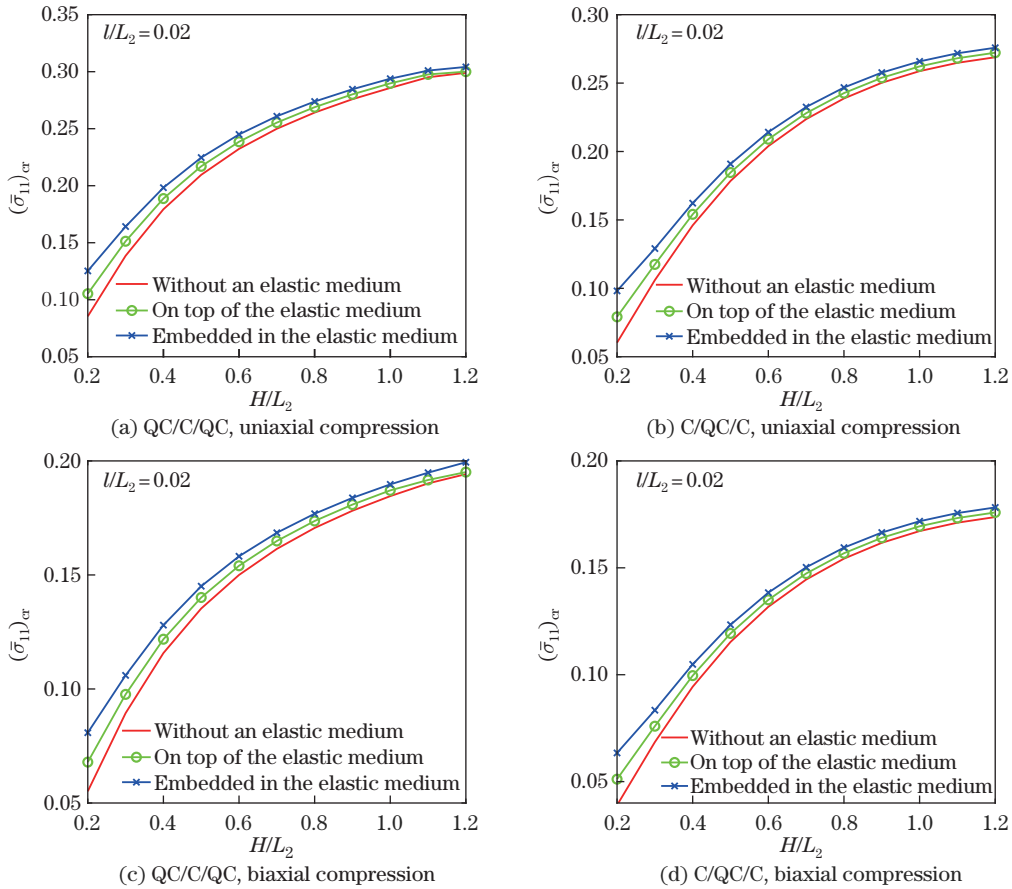

Fig. 8 Variations of the dimensionless critical buckling load of the sandwich QC/C/QC and C/QC/C nanoplates versus the plate thickness (under uniaxial and biaxial compression and with a fixed nonlocal parameter) (color online)

References

[1] SHECHTMAN, D., BLECH, I., GRATIAS, D., and CAHN, J. W. Metallic phase with long-range orientational order and no translational symmetry. *Physical Review Letters*, **53**, 1951–1953 (1984)

[2] BENDERSKY, L. Quasicrystal with one-dimensional translational symmetry and a tenfold rotation axis. *Physical Review Letters*, **55**, 1461–1463 (1985)

[3] CHATTOPADHYAY, K., RANGANATHAN, S., SUBBANNA, G. N., and THANGARAJ, N. Electron microscopy of quasi-crystals in rapidly solidified Al-14% Mn alloys. *Scripta Metallurgica*, **19**, 767–771 (1985)

[4] TSAI, A. P., INOUE, A., and MASUMOTO, T. New decagonal Al-Ni-Fe and Al-Ni-Co alloys prepared by liquid quenching. *Materials Transactions*, *JIM*, **30**, 150–154 (1989)

[5] BINDI, L., YAO, N., LIN, C., HOLLISTER, L. S., ANDRONICOS, C. L., DISTLER, V. V., EDDY, M. P., KOSTIN, A., KRYACHKO, V., and MACPHERSON, G. J. Natural quasicrystal with decagonal symmetry. *Scientific Reports*, **5**, 9111 (2015)

[6] AHN, S. J., MOON, P., KIM, T. H., KIM, H. W., SHIN, H. C., KIM, E. H., CHA, H. W., KAHNG, S. J., KIM, P., and KOSHINO, M. Dirac electrons in a dodecagonal graphene quasicrystal. *Science*, **361**, 782–786 (2018)

[7] LIU, L., LI, Z., LI, Y., and MAO, C. Rational design and self-assembly of two-dimensional, dodecagonal DNA quasicrystals. *Journal of the American Chemical Society*, **141**, 4248–4251 (2019)

[8] CHEN, J. H., CAI, C., and FU, X. J. Decagonal and dodecagonal quasicrystals obtained by molecular dynamics simulations. *Chinese Physics Letters*, **36**, 036101 (2019)

[9] DUBOIS, J. M. Properties and applications of quasicrystals and complex metallic alloys. *Chemical Society Reviews*, **41**, 6760–6777 (2012)

[10] TSAI, A. P. Discovery of stable icosahedral quasicrystal: progress in understanding structure and properties. *Chemical Society Reviews*, **42**, 5352–5365 (2013)

[11] YADAV, T. P. and MUKHOPADHYAY, N. K. Quasicrystal: a low-frictional novel material. *Current Opinion in Chemical Engineering*, **19**, 163–169 (2018)

[12] YU, Z., KUCZERA, P., SOLOGUBENKO, A., SUMIGAWA, T., KITAMURA, T., STEURER, W., and SPOLENAK, R. Superior room-temperature ductility of typically brittle quasicrystals at small sizes. *Nature Communications*, **7**, 12261 (2016)

[13] USTINOV, A. I., MOVCHAN, B. A., and POLISHCHUK, S. S. Formation of nanoquasicrystalline Al-Cu-Fe coatings at electron beam physical vapour deposition. *Scripta Materialia*, **50**, 533–537 (2004)

[14] GALANO, M., MARSH, A., AUDEBERT, F., XU, W., and RAMUNDO, M. Nanoquasicrystalline Al-based matrix/γ-Al_2O_3 nanocomposites. *Journal of Alloys and Compounds*, **643**, S99–S106 (2015)

[15] PEDRAZZINI, S., GALANO, M., AUDEBERT, F., SIEGKAS, P., GERLACH, R., TAGARIELLI, V. L., and SMITH, G. D. W. High strain rate behaviour of nano-quasicrystalline $Al_{93}Fe_3Cr_2Ti_2$ alloy and composites. *Materials Science and Engineering*: *A*, **764**, 138201 (2018)

[16] WEI, D. X. and HE, Z. B. Multilayered sandwich-like architecture containing large-scale faceted Al-Cu-Fe quasicrystal grains. *Materials Characterization*, **111**, 154–161 (2016)

[17] YADAV, T. P., WOELLNER, C. F., SHARIFI, T., SINHA, S. K., QU, L. L., APTE, A., MUKHOPADHYAY, N. K., SRIVASTAVA, O. N., VAJTAI, R., GALVÃO, D. S., TIWARY, C. S., and AJAYAN, P. M. Extraction of two-dimensional aluminum alloys from decagonal quasicrystals. *ACS Nano*, **14**, 7435–7443 (2020)

[18] LIM, C. W. and WANG, C. M. Exact variational nonlocal stress modeling with asymptotic higher-order strain gradients for nanobeams. *Journal of Applied Physics*, **101**, 054312 (2007)

[19] LU, L., GUO, X. M., and ZHAO, J. Z. A unified size-dependent plate model based on nonlocal strain gradient theory including surface effects. *Applied Mathematical Modelling*, **68**, 583–602 (2019)

[20] LI, X. F., GUO, J. H., and SUN, T. Y. Bending deformation of multilayered one-dimensional quasicrystal nanoplates based on the modified couple stress theory. *Acta Mechanica Solida Sinica*, **32**, 785–802 (2019)

[21] LIU, J. J., CHEN, L., XIE, F., FAN, X. L., and LI, C. On bending, buckling and vibration of graphene nanosheets based on the nonlocal theory. *Smart Structures and Systems*, **17**, 257–274 (2016)

[22] LIU, J. J., LI, C., FAN, X. L., and TONG, L. H. Transverse free vibration and stability of axially moving nanoplates based on nonlocal elasticity theory. *Applied Mathematical Modelling*, **45**, 65–84 (2017)

[23] LI, C., LIU, J. J., CHENG, M., and FAN, X. L. Nonlocal vibrations and stabilities in parametric resonance of axially moving viscoelastic piezoelectric nanoplate subjected to thermo-electro-mechanical forces. *Composites Part B*: *Engineering*, **116**, 153–169 (2017)

[24] WAKSMANSKI, N., PAN, E., YANG, L. Z., and GAO, Y. Free vibration of a multilayered one-dimensional quasi-crystal plate. *Journal of Vibration and Acoustics*, **136**, 041019 (2014)

[25] YANG, L. Z., LI, Y., GAO, Y., PAN, E., and WAKSMANSKI, N. Three-dimensional exact electric-elastic analysis of a multilayered two-dimensional decagonal quasicrystal plate subjected to patch loading. *Composite Structures*, **171**, 198–216 (2017)

[26] LI, Y., YANG, L. Z., GAO, Y., and PAN, E. Cylindrical bending analysis of a layered two-dimensional piezoelectric quasicrystal nanoplate. *Journal of Intelligent Material Systems and Structures*, **29**, 2660–2676 (2018)

[27] LI, Y., YANG, L. Z., ZHANG, L. L., and GAO, Y. Three-dimensional exact solution of layered two-dimensional quasicrystal simply supported nanoplates with size-dependent effects. *Applied Mathematical Modelling*, **87**, 42–54 (2020)

[28] WAKSMANSKI, N. and PAN, E. Nonlocal analytical solutions for multilayered one-dimensional quasicrystal nanoplates. *Journal of Vibration and Acoustics*, **139**, 021006 (2017)

[29] ZHANG, L., GUO, J. H., and XING, Y. M. Bending deformation of multilayered one-dimensional hexagonal piezoelectric quasicrystal nanoplates with nonlocal effect. *International Journal of Solids and Structures*, **132**, 132–133 (2018)

[30] GUO, J. H., ZHANG, M., CHEN, W. Q., and ZHANG, X. Y. Free and forced vibration of layered one-dimensional quasicrystal nanoplates with modified couple-stress effect. *Science China-Physics Mechanics and Astronomy*, **63**, 274621 (2020)

[31] GUO, J. H., SUN, T. Y., and PAN, E. Three-dimensional nonlocal buckling of composite nanoplates with coated one-dimensional quasicrystal in an elastic medium. *International Journal of Solids and Structures*, **185**, 272–280 (2020)

[32] ERINGEN, A. C. *Nonlocal Continuum Field Theories*, Springer, New York, 82–87 (2002)

[33] YANG, L. Z., GAO, Y., PAN, E., and WAKSMANSKI, N. An exact solution for a multilayered two-dimensional decagonal quasicrystal plate. *International Journal of Solids and Structures*, **51**, 1737–1749 (2014)

[34] WU, C. P. and LI, W. C. Asymptotic nonlocal elasticity theory for the buckling analysis of embedded single-layered nanoplates/graphene sheets under biaxial compression. *Physica E*, **89**, 160–169 (2017)

[35] FAN, T. Y. Mathematical theory and methods of mechanics of quasicrystalline materials. *Engineering*, **5**, 407–448 (2013)

[36] LEE, J. S. and JIANG, L. Z. Exact electroelastic analysis of piezoelectric laminae via state space approach. *International Journal of Solids and Structures*, **33**, 977–990 (1996)

[37] SOBHY, M. Thermomechanical bending and free vibration of single-layered graphene sheets embedded in an elastic medium. *Physica E*, **56**, 400–409 (2014)

[38] WANG, Q. and WANG, C. M. The constitutive relation and small scale parameter of nonlocal continuum mechanics for modelling carbon nanotubes. *Nanotechnology*, **18**, 075702 (2007)

[39] ANSARI, R. and ROUHI, H. Explicit analytical expressions for the critical buckling stresses in a monolayer graphene sheet based on nonlocal elasticity. *Solid State Communications*, **152**, 56–59 (2012)

[40] PRADHAN, S. C. and MURMU, T. Small scale effect on the buckling of single-layered graphene sheets under biaxial compression via nonlocal continuum mechanics. *Computational Materials Science*, **47**, 268–274 (2010)

[41] CHEN, J. Y., GUO, J. H., and PAN, E. Wave propagation in magneto-electro-elastic multilayered plates with nonlocal effect. *Journal of Sound and Vibration*, **400**, 550–563 (2017)

[42] LI, C., LAI, S. K., and YANG, X. On the nano-structural dependence of nonlocal dynamics and its relationship to the upper limit of nonlocal scale parameter. *Applied Mathematical Modelling*, **69**, 127–141 (2019)

[43] ERINGEN, A. C. On differential equations of nonlocal elasticity and solutions of screw dislocation and surface waves. *Journal of Applied Physics*, **54**, 4703–4710 (1983)

[44] LI, Y., YANG, L. Z., ZHANG, L. L., and GAO, Y. Nonlocal free and forced vibration of multilayered two-dimensional quasicrystal nanoplates. *Mechanics of Advanced Materials and Structures*, **28**, 1216–1226 (2021)

[45] SARRAMI-FOROUSHANI, S. and AZHARI, M. Nonlocal vibration and buckling analysis of single and multi-layered graphene sheets using finite strip method including van der Waals effects. *Physica E*, **57**, 83–95 (2014)

[46] SRINIVAS, S. and RAO, A. K. Bending, vibration and buckling of simply supported thick orthotropic rectangular plates and laminates. *International Journal of Solids and Structures*, **6**, 1463–1481 (1970)